Journal of Materials Chemistry C

ROYAL SOCIETY OF CHEMISTRY

PAPER

View Article Online
View Journal | View Issue

Check for updates

Cite this: J. Mater. Chem. C, 2025, 13, 7678

Design and mesomorphism of a triskelion shape-persistent HBC-TP hybrid: 2,8,14-tris(triphenylen-2-yl)hexabenzocoronene†

Xue Wu,[a] Hang Lin,[a] Xiao-Yan Bai,[a] Ping Hu,[a] Bi-Qin Wang,[a] Ke-Qing Zhao *[a] and Bertrand Donnio *[b]

Received 13th January 2025,
Accepted 8th March 2025

DOI: 10.1039/d5tc00141b

rsc.li/materials-c

A triskelion-shaped mesogen has been synthesized by combining in a single structure, two iconic discotic polycyclic aromatic hydrocarbons (PAHs), namely hexabenzocoronene (HBC), serving as the central core, and three radial mesomorphic triphenylene (TP) subunits sigma-bonded to HBC. The resulting mixed, π-extended oligomer displays a broad temperature range columnar mesophase, characterized by self-sorted columnar stacks of HBC radially fused with three TP-based columns, respectively, evenly distributed within a rectangular 2D lattice (Col_{rec}-*p2mg*). The photophysical properties reveal a wide absorption band that encompasses the combined absorption features of both components, while the emission is predominantly centred on the HBC moiety. Furthermore, the compound demonstrates ambipolar charge transport behaviour, with a pronounced electron-dominant transport.

Introduction

Polycyclic aromatic hydrocarbons (PAHs) form a ubiquitous and extremely diverse class of π-conjugated organic molecules.[1] Primarily composed of condensed benzene and cyclopentadiene rings, PAHs exhibit remarkable variation in size and shape *e.g.* acenes and picenes,[2] rylenes and pyrenes,[3] circumacenes,[4] helicenes *etc.*[5] Their complexity extends to intricate and even contorted topologies,[1,6] alongside numerous geometrical isomers.[7,8] These structural nuances profoundly influence their π–π intermolecular interactions, electronic and optical properties, as well as their aromaticity, chemical reactivity, thermal and photo stability.[9] Their study thus elicits significant interest across various fields, including environmental and health sciences,[10] as well as material engineering,[11] where PAHs are particularly appealing as fundamental building blocks for organic electronics and optoelectronics with applications encompassing flexible electronics, sensors, light and energy storage devices, biomedical imaging, and display technologies.

PAHs, and particularly the emblematic triphenylenes (TPs)[12] and hexabenzocoronenes (HBCs),[13] alongside their π-extended derivatives,[14] have been extensively explored as functional discotic liquid crystal (DLC) materials when aliphatic chains are grafted onto their periphery.[15] This straightforward design enables these molecules to spontaneously stack in one-dimensional columnar structures driven by strong π–π stacking interactions. These columns then self-organize into liquid crystalline two-dimensional networks, mediated by the alkyl chains. Among their distinctive advantages, these materials can be macroscopically aligned into large monodomains, ease processing, and self-heal structural defects due to molecular fluctuations and mobility. These supramolecular networks can persist over a broad temperature range, a critical factor for applications that demand thermal robustness. The potential efficient transport charge carriers along the columns, coupled with tuneable light absorption and emission properties, positions DLC based on TPs and HBCs as attractive candidates for the next-generation organic electronic, optoelectronic, and energy-related devices, offering significant potential for technological breakthroughs.[1,11,16]

Chemical modifications of both the core and periphery of TP and HBC moieites,[17] or their association within complex oligomeric structures,[18,19] have led to the development of a wide range of fascinating molecular architectures. These modifications not only significantly broaden the potential application domains of these materials but also enhance performance of devices in which they are incorporated, enabling advancements across various fields, including organic electronics and optoelectronics. One promising approach involves the use of rigid,

[a] College of Chemistry and Material Science, Sichuan Normal University, Chengdu, 610066, China. E-mail: kqzhao@sicnu.edu.cn
[b] Institut de Physique et Chimie des Matériaux de Strasbourg, UMR 7504 (CNRS-Université de Strasbourg), 67034 Strasbourg, France. E-mail: bdonnio@ipcms.unistra.fr

† Electronic supplementary information (ESI) available: Materials and equipment, detailed synthetic protocols and supplementary schemes, NMR and HMRS spectra, TGA and DSC graphs and tables, S/WAXS diffractograms, tables of indexation and mesophases' parameters, table of photophysical parameters and DFT analysis. See DOI: https://doi.org/10.1039/d5tc00141b

π-extended oligomers – molecules composed of a few repeated PAH monomeric units connected directly by conjugated (σ, π) or metallic bonds,[19] to prevent the interruption of the conjugation, as opposed to the more common flexible oligomers linked by soft spacers.[18] In such hybrid structures, the sequential arrangement of the PAH units and the overall oligomeric topology (linear, branched) will play a key role in determining electronic properties and organization by influencing orbitals' overlaps and stacking interactions (steric hindrance and torsion angle between successive units). To date, only a limited number of such extended conjugated oligomeric discotic systems have been yet synthesized.[19]

In this study, we present the synthesis and detailed investigation of the mesomorphic, electronic and optical properties of an unprecedented π-extended oligomer featuring a distinctive triskelion-like shape.[6] This compound may be considered as a unique subclass of the emerging family of hekate mesogenic materials.[20] This molecule, combining a central HBC core σ-bonded to three radial TP subunits, self-organizes into a broad temperature range columnar rectangular mesophase (Col_{rec}-*p2mg*), displays a wide absorption band that encompasses the combined absorption features of both components, while the emission is predominantly centred on the HBC moiety. Further, it demonstrates ambipolar charge transport behaviour, with electron-dominant transport. This type of materials therefore offers new insights into the design of advanced functional materials with tailored properties for use in a variety of applications, including liquid crystal devices and organic electronics.

Results and discussion

Synthetic procedures

The oligomer, designated as **HBC-3TP**, was synthesized in moderate yields by Suzuki coupling (31%, Scheme 1) between (3,6,7,10,11-pentaalkoxytriphenylene)dioxoborolane (**TP**8/2-Bpin, Scheme S1, ESI†)[21] and 2,8,14-triiodohexabenzo[*bc*,*ef*,*hi*,*kl*,*no*,*qr*]coronene[22] (**HBC-3I**, Scheme S2, ESI†). To enhance the solubility of the oligomer and decrease the transition temperatures, a racemic branched alkyl chain (3,7-dimethyloctyl) was introduced to modify the TP periphery in place of linear *n*-alkyl chains.[13,14] **HBC-3TP** was fully characterized by CHN elemental analysis, ^{1}H and ^{13}C NMR and HRMS (Fig. S1–S11, ESI†).

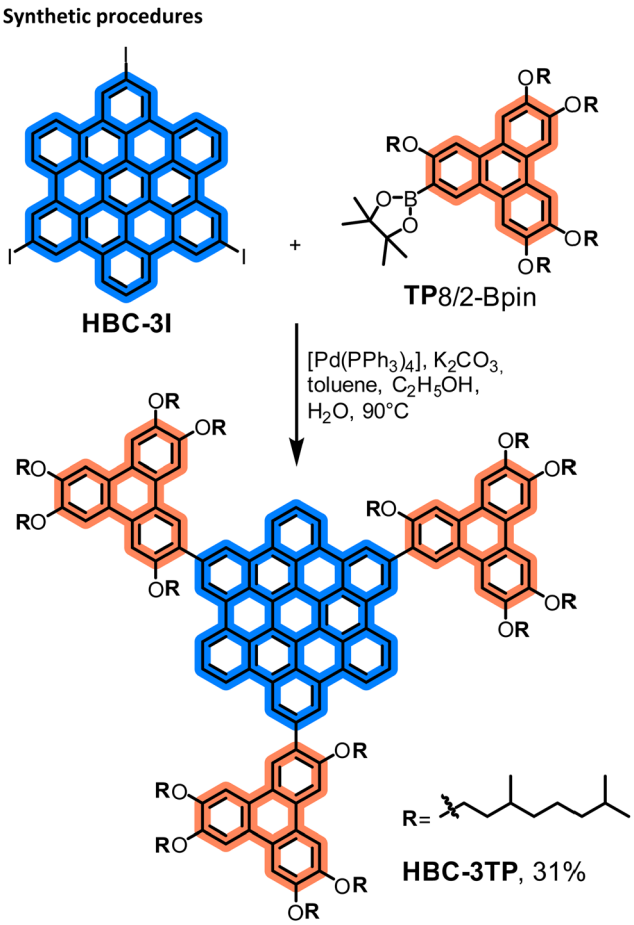

Scheme 1 Synthesis and chemical structure of **HBC-3TP** (the syntheses of **TP**8/2-Bpin and **HBC-3I** are shown in ESI,† Schemes S1 and S2, respectively).

Thermal and liquid crystal properties

Thermogravimetric analysis in dynamic mode (TGA, Fig. 1(a) and Table S1, ESI†) demonstrates the compound's high thermal stability, with a decomposition temperature starting above 330 °C (measured at 5% weigh-loss). This stability allowed for the recording of reversible differential scanning calorimetry (DSC, Fig. 1(b) and Table S2, ESI†) cycles, up to slightly above the isotropization temperature, at 288 °C. After cooling from the isotropic liquid, the compound does not crystallize and remains indefinitely in the mesomorphous state.

Polarized optical microscopy (POM) observations conducted during cooling from the isotropic liquid confirmed the presence of a mesophase, which persisted down to room temperature. Highly colourful and birefringent textures

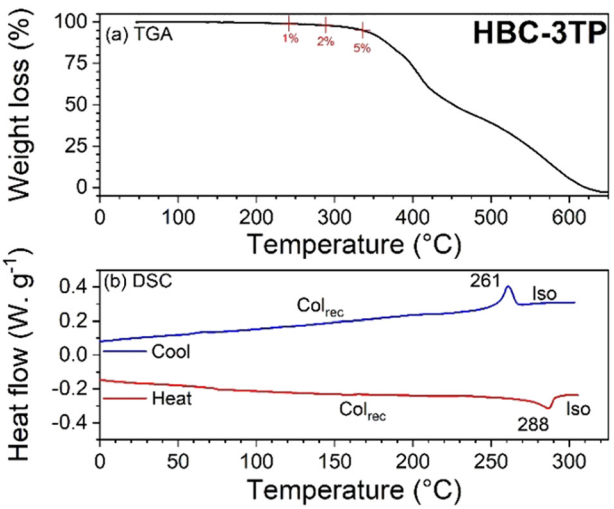

Fig. 1 TGA (a) and DSC (b) curves of **HBC-3TP** (TGA: 1, 2 and 5% correspond to decomposition temperatures at 1, 2 and 5% weight-loss, see also Table S1 (ESI†); DSC: 1st cooling and 2nd heating, blue and red curves, respectively, see also Table S2, ESI†).

exhibiting fern-like and pseudo-focal conic defects could be observed, characteristics of a columnar mesophase (Fig. 2).

Small- and wide-angle X-ray scattering (S/WAXS) patterns were recorded at various temperatures during both heating and cooling cycles to identify the mesophase. During the first heating process, the sample remained stiff until approximately 200 °C (as observed by POM), where it began to soften into the mesomorphic state. Consistently, the S/WAXS patterns showed slightly broaden small-angle peaks (Fig. S12, ESI†), which compromised indexing accuracy. To improve measurement quality, the temperature was increased to 275 °C – the maximum oven temperature – a few degrees Celsius below the isotropic liquid state (Fig. 1), and the sample was held at this temperature for 2–3 minutes before being slowly cooled to 250 °C for X-ray recording. This thermal annealing led to well-resolved X-ray diffraction patterns, which unexpectedly revealed a large number of sharp small-angle reflections, with the first four peaks being notably very intense, and an atypical distribution of the reflection intensities. This small-angle part remains almost unchanged between 250 and 50 °C (Fig. S12, ESI†), *i.e.* peak positions and intensities are almost invariant, which signifies the preservation of lattice size and symmetry. The entire set of reflections could be successfully indexed according to a two-dimensional lattice of rectangular symmetry (Fig. 3 and Fig. S12, Table S3, ESI†). In the wide-angle region, a pronounced pseudo-sharpened peak, increasing with temperature from 3.77 to 4.0 Å corresponding to the π–π stacking between aromatic nuclei in supramolecular columns, h_π, is observed (h_{HBC} and h_{TP} cannot be actually differentiated because their values are very close to each other, $h_\pi \approx h_{HBC} \approx h_{TP}$),[23,24] alongside a wide and strong dispersion peak centred around 5.0 Å corresponding to alkyl chains in the molten state, h_{ch}. **HBC-3TP** thus self-organizes into a rectangular columnar mesophase, with two columnar motifs ($N_{col} = 2$) per lattice.

The numerous reflections, systematically observed across all temperatures (Fig. S12, ESI†), indicate a long-range, two-dimensional expansion of the rectangular lattice and the presence of well-defined aliphatic–aromatic interfaces, creating distinctly segregated regions of high electronic density interspersed with a low-electronic-density aliphatic continuum. The atypical distribution of the reflection intensities aligns with a low-symmetry alternating electronic density pattern within the rectangular lattice. These distinctive features are attributed to the molecule's unique triskelion geometry and efficient molecular self-sorting between HBC core, TP moieties and chains, indicative of a highly specific supramolecular organisation.

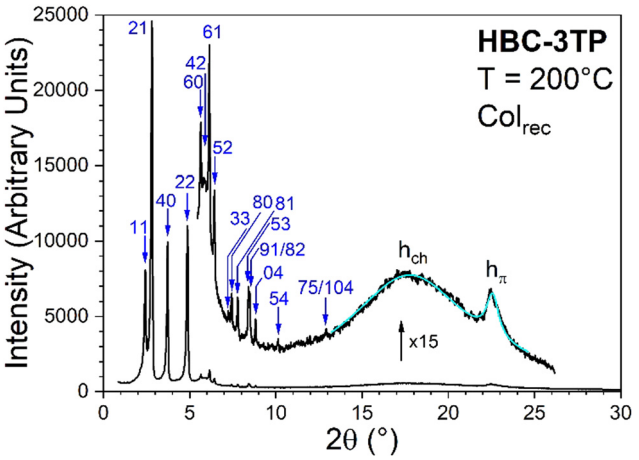

Fig. 3 S/WAXS pattern of **HBC-3TP** recorded on cooling at 200 °C, showing the peaks indexation with *hk* Miller indices (see also Table S3, ESI†).

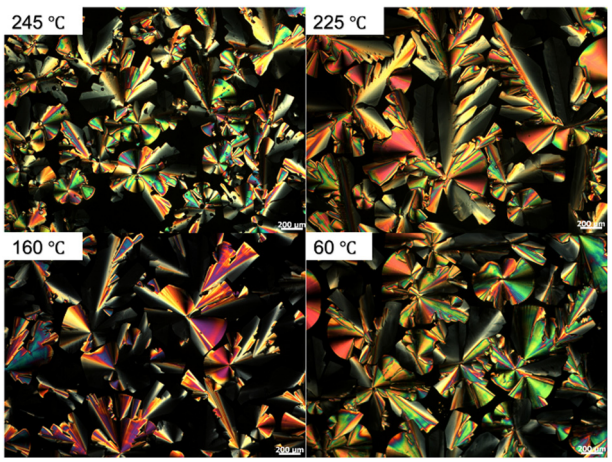

Fig. 2 POM photomicrographs of **HBC-3TP**, obtained on slow cooling from the isotropic liquid at different temperatures.

The induction of the columnar mesophase is primarily driven by the segregation between aromatic and aliphatic components, along with the natural tendency of the large HBC cores and the smaller TP cores to stack into distinct "HBC-like" and "TP-like" one-dimensional columns, respectively. This differentiation arises from the specific molecule's triskelion-like shape (see DFT, Fig. S15, ESI†), the significant size disparity between the two aromatic cores diameters ($\phi_{HBC} > \phi_{TP}$) and stoichiometry (HBC : TP 1 : 3), and the presence of aliphatic chains exclusively on the TP units, which make the formation of mixed HBC-TP stacks highly unlikely. The parameters and cross-sectional area of the rectangular lattice (a = 94.92 Å, b = 39.45 Å, S = 3745 Å^2 at 200 °C, Table S3, ESI†) are compatible with the accommodation of two complete molecules ($N_{col} = N_{mol} = 2$) within the elementary cell, as confirmed by the calculated values of the average molecular thickness h_{mol} (ratio between estimated molecular volume[25,26] and the lattice area, see Table S4, ESI†) ranging around those of the stacking distance. These values, although slightly smaller than h_π, particularly at low temperature, still vary as the stacking distance, support the self-sorting of HBC and TP stacks into a "multicolumnar" mesophase. The mean stacking distance between π-conjugated cores, h_π, was found to increase slightly with temperature from *ca.* 3.77 Å at 50 °C to 4.00 Å at 250 °C, and is accompanied by the widening of the scattering maxima, consistent with reduced correlation lengths (Table S4 and Fig. S11, ESI†). This temperature-dependent axial expansion is attributed to the increasing disorder along the columns, due likely to the fluctuations of the lateral triphenylene moieties relative to the HBC core and the lattice plane (Fig. S14 and Table S4, ESI†). Concurrently, upon cooling, as molecular motion and

volume reduce, the stacking distance, h_π, decreases, and the rotation of the lateral TP segments becomes restricted, effectively locking the stacking, consistent with the solidification of the aliphatic chains.

The reduced symmetry of the rectangular lattice implies that the columnar cross-section is not uniform (*i.e.*, not circular, but also not elliptical), and is likely stemming from the shape-persistent molecular architecture of **HBC-3TP**, *i.e.* the orthogonal projection of the molecule on the lattice plane. An alternating 180° molecular stacking (*i.e.*, AB-like stacking), which could produce cylindrical columns on average, is highly improbable due to the inherent incompatibility between the aliphatic chains and aromatic TP units. Consequently, the columnar cross-section likely retains intrinsic aspects of the unique three-fold triskelion molecular shape.

Several plausible supramolecular organizations for the triskelion molecule within the lattice can be envisioned, depending on the mutual arrangement of the molecules (three-fold columnar cross-sections). Among the two molecules present in the rectangular cell, one is positioned at the lattice corners and aligns along either of the two lattice axes, *a* and *b* (Fig. 4(a)–(d), respectively). The second molecule is located at the centre of the lattice and can adopt either a parallel (Fig. 4(a) and (c)) or an antiparallel (Fig. 4(b) and (d)) orientation relative to the corners' molecules. The parallel orientation (Fig. 4(a) and (c)) leads to the plane group *cm*,[27] whilst the antiparallel mode (Fig. 4(b) and (d)) generates the plane group *p2mg*.[27] The *cm* option is not consistent with the reflections' indexation due to the presence of forbidden reflections (general conditions: $hk{:}h + k = 2n$, $h0{:}h = 2n$, $0k{:}k = 2n$), and thus the parallel configurations can be excluded. Given this, the most likely plane group is thus *p2mg*, although, at this stage, it is not possible to distinguish between the two antiparallel configurations shown in Fig. 4(b) and (d). Although, the distribution of the aliphatic chains shown in Fig. 4(b) appears more uniform and equilibrated compared to the configuration in Fig. 4(d), where there is a clear alternation between regions of high and low chains density, the more balanced distribution in Fig. 4(b) suggests that this arrangement is the most likely and stable configuration. Thus, based on this observation, the arrangement depicted in Fig. 4(b) is considered the most probable.

The reduction in mesophase symmetry is thus consistent with the intrinsic C_3 symmetry of **HBC-3TP**, which governs the arrangement of the columns and results in an inhomogeneous electron density distribution within the lattice. This inhomogeneity is reflected in the atypical distribution of reflection intensities, similar to what has been observed in some other multicolumnar systems.[19] This columnar Col_{rec}-*p2mg* phase then consists of central HBC-like columns radially fused with three TP-like columns, the concerted molecular orientations being constrained by the voluminous aliphatic matrix surrounding the columns (approximately 75–80% of the total molecular volume, Table S4, ESI†).

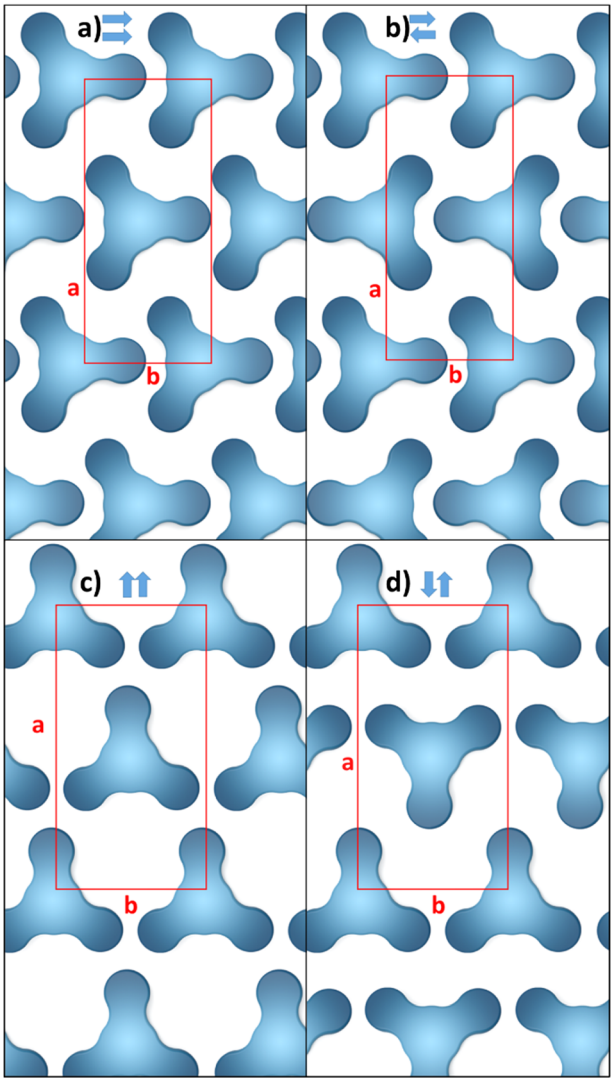

Fig. 4 Schematic proposals for the supramolecular organization of **HBC-3TP** in the Col_{rec} phase (N_{mol} = 2). Various views of the possible rectangular lattices with parallel ((a), (c): plane group *cm*) and antiparallel ((b), (d): plane group *p2mg*) molecular orientations (blue arrows) along lattice *b*-axis (a), (b) and *a*-axis (c), (d), respectively; the trifold blue shape represents a schematic of the **HBC-3TP** molecule (molecular representation: HBC: illuminated centres, TP: dark circles); molten chains (not represented) in white continuum (see also Fig. S13, ESI†).

Optical properties

The optical properties of **HBC-3TP** were also investigated in solution and thin film (Fig. 5 and Fig. S18, Table S7, ESI†). The absorption spectrum displays two main absorption maxima appearing at *ca.* 282 and 370 nm, respectively. The peak near 280 nm can be attributed to the absorption of the TP moiety. UV-Vis absorption spectra of solutions of **TP6** in dichloromethane and THF, show a strong absorption maximum at 279 nm, corresponding to an S0 → S4 transition,[28] with a molar absorption coefficient (ε) around 1×10^5 dm^3 mol^{-1} cm^{-1} (Table S5, ESI†). Additionally, there is a shoulder at *ca.* 309 nm, which corresponds to an S0 → S3 transition. The signal at lower energy (λ_{abs} = 370 nm) is attributed to the HBC moiety, with the model **HBC** compound absorbing at 352 nm. Previous reports on the absorption spectra of dilute solutions of hexabenzocoronenes indicate a highly structured pattern, which typically arises from

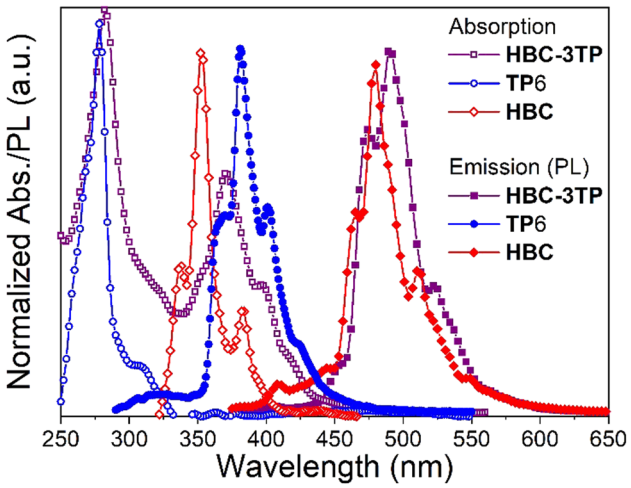

Fig. 5 Photophysical properties of **HBC-3TP** compared with optical properties of model compounds, **TP**6 (2,3,6,7,10,11-hexakis(hexyloxy)-triphenylene) and **HBC** (hexabenzo[*bc*,*ef*,*hi*,*kl*,*no*,*qr*]coronene). UV-vis absorption and fluorescence emission in THF ($c = 10^{-6}$ mol L^{-1}).

various electronic transitions and/or vibrational progressions occurring in the system. The redshift of this signal is attributed to the extension of the conjugation of the TP units with the central HBC.

The photoluminescence spectrum of **HBC-3TP** exhibits a single intense emission peak with a maximum at *ca.* 489 nm, which closely coincides with the fluorescence of the model **HBC** compound (λ_{em} = 480 nm). Quite remarkably for this hybrid π-oligomer, only the emission from the HBC subunit is detected, regardless of the excitation wavelength used, *i.e.*, whether this excitation is directed at the TP subunit (λ_{em} = 275 nm) or the HBC part (λ_{em} = 375 nm). This can be due to an efficient energy transfer from the TP to the HBC unit, or alternatively by the absorption of the TP emission (at 375 nm) by the HBC subunit, as there is significant overlap between the TP emission and HBC absorption spectra. This unexpected interplay between both TP and HBC units lends to an intriguing fluorescent system, highlighting the photophysical potential of such hybrid oligomers.

In thin film, the single luminescence maximum of **HBC-3TP** is redshifted (Fig. S18, ESI† $\lambda_{em,max}$ = 542 nm) by about 50 nm compared to its solution emission. The observed emission shift is also accompanied by a significant reduction of the luminescence intensity and thus of the quantum yield (QY), which drops from 23.66% in solution to just 2.51% in the thin film (Table S7, ESI†). This shift in emission behaviour can be attributed to the aggregation-caused quenching (ACQ) phenomenon which likely results from the formation of intermolecular H-type aggregates in thin film. This is supported by S/WAXS data and consistent with the proposed model of the Col_{rec} mesophase.

The oxidation potential of **HBC-3TP** determined by cyclic voltammetry (CV, Fig. S19, ESI†) gave a measured HOMO energy level of −5.33 eV, which is quite close to the HOMO calculated by DFT of −5.28 eV (Tables S6–S8, ESI†). As the reduction potential was not obtained directly, the optical energy gap was used to estimate the LUMO energy level, resulting in a value of approximately −2.45 eV. This value differs quite substantially from the theoretically predicted LUMO value of −1.89 eV. This discrepancy between experimental and computational results may be due to solvation effects, computational approximations, or experimental limitations.

Charge carrier mobility

Carrier mobility plays an essential role in organic semiconductor applications, directly affecting device performance. The space charge limited current (SCLC) method was used to investigate the carrier transport properties of **HBC-3TP**.[29] To measure both hole and electron mobilities, hole-only devices (ITO/PEDOT:PSS/**HBC-3TP** (119 nm)/Au) and electron-only devices (ITO/ZnO/**HBC-3TP** (113 nm)/PFN-Br/Ag) were fabricated. The sample films were thermally annealed at 241 °C to optimize charge transport, and gave hole and electron mobilities of 8.22×10^{-5} cm^2 V^{-1} S^{-1} and 5.67×10^{-3} cm^2 V^{-1} S^{-1}, respectively (Fig. 6 and Fig. S20, ESI†). The enhancement in carrier mobility can be attributed to improved molecular ordering within the thin films: as **HBC-3TP** possesses a room temperature Col_{rec} mesophase, the spin-coated films were thermally annealed near the isotropic temperature and then slowly cooled down to room temperature. This process facilitated the formation of highly ordered homeotropic columnar assembly regions, which significantly improved charge carrier mobility.

HBC-3TP thus exhibits ambipolar charge transport behaviour. The electron mobility is significantly higher than the hole mobility, with an electron-to-hole mobility ratio of approximately 70 : 1. S/WAXS analysis revealed that **HBC-3TP** self-organizes into an ordered, highly segregated columnar structure consisting of a central HBC column surrounded by radially arranged TP-based columns. The TP units, functionalized with five peripheral alkoxy chains, are electron-rich and typically facilitate hole transport. In contrast, the graphene-like HBC

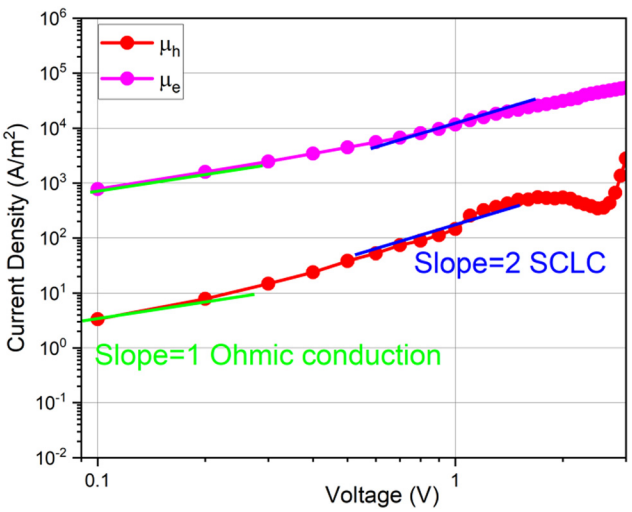

Fig. 6 *I*–V curves of **HBC-3TP** in SCLC devices: electron mobility (μ_e), hole mobility (μ_h).

core, substituted with three TP moieties, is more favourable for electron transport. The ambipolar behaviour of **HBC-3TP** is consistent with previously reported results on HBC- and TP-based discotic liquid crystals.[17–21,30,31] This pronounced electron-dominant transport behaviour highlights the influence of molecular design and self-organization on carrier mobility.

Conclusions

Thus, as expected, this triskelion-shaped oligomeric compound, composed of two of the most popular discotic components, is mesomorphic and self-organizes into a rectangular columnar phase of reduced symmetry, characterized by the *p*2*mg* planar group. The supramolecular organization consists of central HBC-like columns radially fused with three TP-like columns positioned at the corners and centre of the rectangular lattice, with antiparallel molecular orientations along the lattice axes. The photophysical properties reveal a wide absorption band that encompasses the combined absorption features of both components, while the emission is predominantly centred on the HBC moiety. Furthermore, the compound demonstrates ambipolar charge transport behaviour, with a pronounced electron-dominant transport. The segregated HBC columns are playing the role of electron transport channel while the TP columns as the hole drift pass-way, as demonstrated by SCLC and CV measurements and supported by DFT computational studies. This type of molecular hybrid systems therefore offers new insights into the design of attractive advanced functional materials with tailored properties for use in a variety of applications, including liquid crystal devices and organic electronics.

Author contributions

Conceptualization, K.-Q. Z. and B. D.; methodology, K.-Q. Z. and B. D.; formal analysis, X. W., H. L., X.-Y. B., K.-Q. Z. and B. D.; investigation, X. W., H. L. and K.-X. Z. and X.-Y. B.; data curation, K.-Q. Z. and B. D.; writing – original draft preparation, K.-Q. Z. and B. D.; writing – review and editing, K.-Q. Z. and B. D.; supervision, K.-Q. Z.; funding acquisition, K.-Q. Z., X.-Y. B., P. H. and B.-Q. W. All authors have read and agreed to the published version of the manuscript.

Data availability

All data that supports the findings of this study is available in the published article and/or the ESI† to this article.

Conflicts of interest

There are no conflicts to declare.

Acknowledgements

The authors thank the National Natural Science Foundation of China for funding (grant numbers: 22101193, 51773140, 51973143, 21772135). BD thanks the CNRS and the University of Strasbourg for constant support.

Notes and references

1 M.-W. Wang, W. Fan, X. Li, Y. Liu, Z. Li, W. Jiang, J. Wu and Z. Wang, *ACS Nano*, 2023, **17**, 20734–20752; Q. Li, Y. Zhang, Z. Xie, W. Zhen, H. Hu and J. Dong, *J. Mater. Chem. C*, 2022, **10**, 2411–2430; Y. Wang, B. Liu, C. W. Koh, X. Zhou, H. Sun, J. Yu, K. Yang, H. Wang, Q. Liao, H. Y. Woo and X. Gui, *Adv. Energy Mater.*, 2019, **9**, 18003976; X.-Y. Wang, X. Yao and K. Müllen, *Sci. China Chem.*, 2019, **62**, 1099–1144; V. Vij, V. Bhalla and M. Kumar, *Chem. Rev.*, 2016, **116**, 9565–9627; F. Dötz, J. Diedrich Brand, S. Ito, L. Gherghel and K. Müllen, *J. Am. Chem. Soc.*, 2000, **122**, 7707–7717.

2 J. E. Anthony, *Angew. Chem., Int. Ed.*, 2008, **47**, 452–483; R. A. Pascal, Jr., *Chem. Rev.*, 2006, **106**, 4809–4819.

3 T. M. Figueira-Duarte and K. Müllen, *Chem. Rev.*, 2011, **111**, 7260–7314.

4 Y. Zou, X. Hou, H. Wei, J. Shao, Q. Jiang, L. Ren and J. Wu, *Angew. Chem., Int. Ed.*, 2023, **62**, e202301041; X.-H. Ma, X. Gao, J.-Y. Chen, M. Cao, Q. Dai, Z.-K. Jia, Y.-B. Zhou, X.-J. Zhao, C. Chu, G. Liu and Y.-Z. Tan, *J. Am. Chem. Soc.*, 2024, **146**, 2411–2418.

5 T. Mori, *Chem. Rev.*, 2021, **121**, 2373–2412; M. Gingras, *Chem. Soc. Rev.*, 2013, **42**, 968–1006; M. Rickhaus, M. Mayor and M. Juríček, *Chem. Soc. Rev.*, 2016, **45**, 1542–1556.

6 C. M. Cruz, I. R. Márquez, S. Castro-Fernández, J. M. Cuerva, E. Maçôas and A. G. Campaña, *Angew. Chem., Int. Ed.*, 2019, **58**, 8068–8072; M. Ball, Y. Zhong, Y. Wu, C. Schenck, F. Ng, M. Steigerwald, S. Xiao and C. Nuckolls, *Acc. Chem. Res.*, 2015, **48**, 267–276; B. A. G. Hammer and K. Müllen, *Chem. Rev.*, 2016, **116**, 2103–2140.

7 G. Brinkmann, G. Caporossi and P. Hansen, *J. Chem. Inf. Comput. Sci.*, 2003, **43**, 842–851; G. Brinkmann, C. Grothaus and I. Gutman, *J. Math. Chem.*, 2007, **42**, 909–924.

8 W. Matsuoka, H. Ito, D. Sarlah and K. Itami, *Nat. Commun.*, 2021, **12**, 3940.

9 M. D. Watson, A. Fechtenkötter and K. Müllen, *Chem. Rev.*, 2001, **101**, 1267–1300.

10 B. Mou, G. Gong and S. Wu, *Chemosphere*, 2023, **341**, 140017; H. Zhou, X. Gao, S. Wang, Y. Zhang, F. Coulon and C. Cai, *Int. J. Environ. Res. Public Health*, 2023, **20**, 1766; X.-H. Ma, X. Gao, J.-Y. Chen, M. Cao, Q. Dai, Z.-K. Jia, Y.-B. Zhou, X.-J. Zhao, C. Chu, G. Liu and Y.-Z. Tan, *J. Am. Chem. Soc.*, 2024, **146**, 2411–2418.

11 Y. Wang, B. Liu, C. W. Koh, X. Zhou, H. Sun, J. Yu, K. Yang, H. Wang, Q. Liao, H. Y. Woo and X. Gui, *Adv. Energy Mater.*, 2019, **9**, 18003976.

12 S. Kumar Pal, S. Setia, B. S. Avinash and S. Kumar, *Liq. Cryst.*, 2013, **40**, 1769–1816; N. Boden, R. C. Borner, R. J. Bushby, A. N. Cammidge and M. V. Jesudason, *Liq. Cryst.*, 1993, **15**, 851–858; S. Kumar, *Liq. Cryst.*, 2004, **31**, 1037–1059; A. Shah, D. P. Singh, B. Duponchel, F. Krasinski, A. Daoudi, S. Kumar and R. Douali, *J. Mol. Liq.*, 2021, **342**, 117353.

13 J. Wu, W. Pisula and K. Müllen, *Chem. Rev.*, 2007, **107**, 718–747; W. Pisula, X. Feng and K. Müllen, *Adv. Mater.*, 2010, **22**, 3634–3649.

14 P. T. Lynett and K. E. Maly, *Org. Lett.*, 2009, **11**, 3726–3729; T. Yatabe, M. A. Harbison, J. D. Brand, M. Wagner, K. Müllen, P. Samori and J. P. Rabe, *J. Mater. Chem.*, 2000, **10**, 1519–1525; K.-Q. Zhao, M. Jing, L.-L. An, J.-Q. Du, Y.-H. Wang, P. Hu, B.-Q. Wang, H. Monobe, B. Heinrich and B. Donnio, *J. Mater. Chem. C*, 2017, **5**, 669–682; Z. Tomović, M. D. Watson and K. Müllen, *Angew. Chem., Int. Ed.*, 2004, **43**, 755–758; W. Pisula, Z. Tomović, C. Simpson, M. Kastler, T. Pakula and K. Müllen, *Chem. Mater.*, 2005, **17**, 4296–4303; S. Xiao, M. Myers, Q. Miao, S. Sanaur, K. Pang, M. L. Steigerwald and C. Nuckolls, *Angew. Chem., Int. Ed.*, 2005, **44**, 7390–7394; Y. Hanai, M. Jalilur Raman, J. Yamakawa, M. Takase, T. Nishinaga, M. Hasegawa, K. Kamada and M. Iyoda, *Chem. – Asian J.*, 2011, **6**, 2940–2945; M. G. Schwab, T. Qin, W. Pisula, A. Mavrinskiy, X. Feng, M. Baumgarten, H. Kim, F. Laquai, S. Schuh, R. Trattnig, E. J. W. List and K. Müllen, *Chem. – Asian J.*, 2011, **6**, 3001–3010; L. Zhang, H. Gopee, D. L. Hughes and A. C. Cammidge, *Chem. Commun.*, 2010, **46**, 4255–4257; E. M. García-Frutos, A. Omenat, J. Barberá, J. L. Serrano and B. Gómer-Lor, *J. Mater. Chem.*, 2011, **21**, 6831–6836; C. Romero, D. Peña, D. Pérez and E. Guitián, *Chem. – Eur. J.*, 2006, **12**, 5677–5684.

15 A. Gowda, M. Kumar and S. Kumar, *Liq. Cryst.*, 2017, **44**, 1990–2017; X. Feng, W. Pisula and K. Müllen, *Pure Appl. Chem.*, 2009, **81**, 2203–2224; T. Wöhrle, I. Wurzbach, J. Kirres, A. Kostidou, N. Kapernaum, J. Litterscheidt, J. C. Haenle, P. Staffeld, A. Baro, F. Giesselmann and S. Laschat, *Chem. Rev.*, 2016, **116**, 1139–1241; B. R. Kaafarani, *Chem. Mater.*, 2011, **23**, 378–396.

16 M. Kumar and S. Kumar, *Polym. J.*, 2017, **49**, 85–111; H. Seyler, B. Purushothaman, D. J. Jones, A. B. Holmes and W. W. H. Wong, *Pure Appl. Chem.*, 2012, **84**, 1047–1067; X. Feng, V. Marcon, W. Pisula, M. R. Hansen, J. Kirkpatrick, F. Grozema, D. Adrienki, K. Kremer and K. Müllen, *Nat. Mater.*, 2009, **8**, 421–426.

17 S. Setia and S. Kumar Pal, *ChemistrySelect*, 2016, **1**, 880–885; S. Ito, M. Wehmeier, J. D. Brand, C. Kübel, R. Epsch, J. P. Rabe and K. Müllen, *Chem. – Eur. J.*, 2000, **6**, 4327–4342; B. Alameddine, O. F. Aebischer, B. Heinrich, D. Guillon, B. Donnio and T. A. Jenny, *Supramol. Chem.*, 2014, **26**, 125–137; A. Fechtenkötter, N. Tchebotareva, M. Watson and K. Müllen, *Tetrahedron*, 2001, **57**, 3769–3783; Y. Wu, W. Zhang, Q. Peng, C. K. Ran, B. Q. Wang, P. Hu, K. Q. Zhao, C. Feng and S. K. Xiang, *Org. Lett.*, 2018, **20**, 2278–2281; N. Boden, R. J. Bushby, Z. B. Lu and A. N. Cammidge, *Liq. Cryst.*, 1999, **26**, 495–499; M. Ichihara, H. Suzuki, B. Mohr and K. Ohta, *Liq. Cryst.*, 2007, **34**, 401–410; M. T. Allen, S. Diele, K. D. M. Harris, T. Hegmann, B. M. Kariuki, D. Lose, J. A. Preece and C. Tschierske, *J. Mater. Chem.*, 2001, **11**, 302–311; A. N. Cammidge and H. Gopee, *J. Mater. Chem.*, 2001, **11**, 2773–2783; X. Feng, W. Pisula, M. Ai, S. Gröper, J. P. Rabe and K. Mullen, *Chem. Mater.*, 2008, **20**, 1191–1193; Q. Zhang, P. Prins, S. C. Jones, S. Barlow, T. Kondo, Z. An, L. D. A. Siebbeles and S. R. Marder, *Org. Lett.*, 2005, **7**, 5019–5022; S. Setia, S. Kumar, D. Adhikari and S. Kumar Pal, *Liq. Cryst.*, 2019, **46**, 430–441; M.-M. Zhou, J. He, H.-M. Pan, Q. Zeng, H. Lin, K.-Q. Zhao, P. Hu, B.-Q. Wang and B. Donnio, *Chem. – Eur. J.*, 2023, **29**, e202301829.

18 T. Plesnivy, H. Ringsdorf, P. Schuhmacher, U. Nutz and S. Diele, *Liq. Cryst.*, 1995, **18**, 185–190; N. C. Maliszewskyj, P. A. Heiney, J. Y. Josefowicz, T. Plesnivy, H. Ringsdorf and P. Schuhmacher, *Langmuir*, 1995, **11**, 1666–1674; N. Boden, R. J. Bushby, A. N. Cammidge, A. El-Mansoury, P. S. Martina and Z. Lu, *J. Mater. Chem.*, 1999, **9**, 1391–1402; L. Zhi, J. Wu and K. Müllen, *Org. Lett.*, 2005, **7**, 5761–5764; A. Zelcer, B. Donnio, C. Bourgogne, F. D. Cukiernik and D. Guillon, *Chem. Mater.*, 2007, **19**, 1992–2006; K.-Q. Zhao, L.-L. An, X.-B. Zhang, W.-H. Yu, P. Hu, B.-Q. Wang, J. Xu, Q.-D. Zeng, H. Monobe, Y. Shimizu, B. Heinrich and B. Donnio, *Chem. – Eur. J.*, 2015, **21**, 10379–10390; E. Beltran, M. Garzoni, B. Feringan, A. Vancheri, J. Barbera, J. L. Serrano, G. M. Pavan, R. Gimenez and T. Sierra, *Chem. Commun.*, 2015, **51**, 1811–1814; V. Conejo-Rodriguez, B. Donnio, B. Heinrich, R. Termine, A. Golemme and P. Espinet, *J. Mater. Chem. C*, 2023, **11**, 1435–1447; Y. Xiao, X. Su, L. Sosa-Vargas, E. Lacaze, B. Heinrich, B. Donnio, D. Kreher, F. Mathevet and A.-J. Attias, *CrystEngComm*, 2016, **18**, 4787–4798.

19 J. Wu, M. D. Watson, N. Tchebotareva, Z. Wang and K. Müllen, *J. Org. Chem.*, 2004, **69**, 8194–8204; W. W. H. Wong, D. J. Jones, C. Yan, S. E. Watkins, S. King, S. A. Haque, X. Wen, K. P. Ghiggino and A. B. Holmes, *Org. Lett.*, 2009, **11**, 975–978; D. Rausch and C. Lambert, *Org. Lett.*, 2006, **8**, 5037–5040; A. O. Alsahli and A. N. Cammidge, *Eur. J. Org. Chem.*, 2022, e202200990; H. Lin, K.-X. Zhao, M. Jing, X.-H. Long, K.-Q. Zhao, P. Hu, B.-Q. Wang, P. Lei, Q.-D. Zeng and B. Donnio, *J. Mater. Chem. C*, 2022, **10**, 14453–14470; R. Chico, C. Dominguez, B. Donnio, B. Heinrich, S. Coco and P. Espinet, *Cryst. Growth Des.*, 2016, **16**, 6984–6991; L. Tao, Y. Xie, K.-X. Zhao, P. Hu, B.-Q. Wang, K.-Q. Zhao and X.-Y. Bai, *New J. Chem.*, 2024, **48**, 12006–12014; J. Ramakrishna, L. Karunakaran, S. V. Kumar Paneer, A. Mithun Chennamkulam, V. Subramanian, S. Dutta and P. Venkatakrishnan, *Eur. J. Org. Chem.*, 2020, 662–673; A. Idelson, C. Sterzenbach, S. S. Jester, C. Tschierske, U. Baumeister and S. Höger, *J. Am. Chem. Soc.*, 2017, **139**, 4429–4434.

20 M. Lehmann, *Chem. – Eur. J.*, 2009, **15**, 3638–3651; M. Lehmann, *Top. Curr. Chem.*, 2012, **318**, 193–224; H. Deter, M. Lehmann and H. Meier, *Materials*, 2010, 3218–3330.

21 C. Zeng, P. Hu, B. Wang, W. Fang and K.-Q. Zhao, *Chin. J. Org. Chem.*, 2023, **43**, 3287–3296.

22 J. Wu, M. Baumgarten, M. G. Debije, J. M. Warman and K. Müllen, *Angew. Chem., Int. Ed.*, 2004, **43**, 5331–5335.

23 R. Goddard, M. W. Haenel, W. C. Herndon, C. Krüger and M. Zander, *J. Am. Chem. Soc.*, 1995, **117**, 30–41.

24 J. C. Collings, K. P. Roscoe, R. L. Thomas, A. S. Batsanov, L. N. Stimson, J. A. K. Howard and T. B. Marder, *New J. Chem.*, 2001, **25**, 1410–1417; T. L. Andresen, F. C. Krebs, N. Thorup and K. Bechgaard, *Chem. Mater.*, 2000, **12**, 2428–2433.

25 B. Donnio, B. Heinrich, H. Allouchi, J. Kain, S. Diele, D. Guillon and D. W. Bruce, *J. Am. Chem. Soc.*, 2004, **126**, 15258–15268.

26 Molecular volumes were calculated by the sum of partial volumes $V_{mol} = V_{ar} + V_{ch}$, with V_{ar}, the volume of the aromatic part deduced from reported single crystal structures of reference compounds *i.e.* HBC – ref. 23 – and TP – ref. 24, and V_{ch}, the volume of the chains;[25] $h_{mol} = N_{mol}V_{mol}/S$ Å, with $N_{mol} = 2$, number of molecules per lattice, and S, the rectangular lattice cross-section.

27 *International Tables for Crystallography Volume A: Space-group symmetry*, ed. M. I. Aroyo, John Wiley & Sons, 2nd edn, 2016 (ISBN: 978-0-470-97423-0).

28 D. Markovitsi, A. Germain, P. Millie, P. Lecuyer, L. Gallos, P. Argyrakis, H. Bengs and H. Ringsdorf, *J. Phys. Chem.*, 1995, **99**, 1005–1017.

29 R. De, J. De, S. P. Gupta, I. Bala, Ankita, Tarun, U. K. Pandey and S. K. Pal, *J. Mater. Chem. C*, 2023, **11**, 980–985.

30 A. M. van de Craats, J. M. Warman, A. Fechtenkötter, J. D. Brand, M. A. Harbison and K. Müllen, *Adv. Mater.*, 1999, **11**, 1469–1472.

31 H. Monobe, Y. Shimizu, S. Okamoto and H. Enomoto, *Mol. Cryst. Liq. Cryst.*, 2007, **476**, 31/[277]–41/[287].